Bi-directional series-parallel elastic actuator and overlap of the actuation layers

2016 Bioinspir. Biomim. 11 016005

(http://iopscience.iop.org/1748-3190/11/1/016005)

Bioinspiration & Biomimetics

OPEN ACCESS

RECEIVED
2 September 2015

REVISED
18 December 2015

ACCEPTED FOR PUBLICATION
22 December 2015

PUBLISHED
26 January 2016

PAPER

Bi-directional series-parallel elastic actuator and overlap of the actuation layers

Raphaël Furnémont[1], **Glenn Mathijssen**[1,2], **Tom Verstraten**[1], **Dirk Lefeber**[1] **and Bram Vanderborght**[1]

[1] Robotics and Multibody Mechanics (R&MM), Vrije Universiteit Brussel (VUB), Pleinlaan 2, B-1050 Brussels, Belgium
[2] Centro E.Piaggio of the University of Pisa, Italy

E-mail: rfurnemo@gmail.com

Keywords: series parallel elastic actuator, compliant actuators, robotics, intermittent mechanism, self-closing mechanism, variable recruitment

Abstract

Several robotics applications require high torque-to-weight ratio and energy efficient actuators. Progress in that direction was made by introducing compliant elements into the actuation. A large variety of actuators were developed such as series elastic actuators (SEAs), variable stiffness actuators and parallel elastic actuators (PEAs). SEAs can reduce the peak power while PEAs can reduce the torque requirement on the motor. Nonetheless, these actuators still cannot meet performances close to humans. To combine both advantages, the series parallel elastic actuator (SPEA) was developed. The principle is inspired from biological muscles. Muscles are composed of motor units, placed in parallel, which are variably recruited as the required effort increases. This biological principle is exploited in the SPEA, where springs (layers), placed in parallel, can be recruited one by one. This recruitment is performed by an intermittent mechanism. This paper presents the development of a SPEA using the MACCEPA principle with a self-closing mechanism. This actuator can deliver a bi-directional output torque, variable stiffness and reduced friction. The load on the motor can also be reduced, leading to a lower power consumption. The variable recruitment of the parallel springs can also be tuned in order to further decrease the consumption of the actuator for a given task. First, an explanation of the concept and a brief description of the prior work done will be given. Next, the design and the model of one of the layers will be presented. The working principle of the full actuator will then be given. At the end of this paper, experiments showing the electric consumption of the actuator will display the advantage of the SPEA over an equivalent stiff actuator.

1. Introduction

Several novel applications such as prostheses, exoskeletons or running robots require higher performance than what the current actuation technology can provide. For these applications the development of actuators with higher torque to weight ratio and efficiency is a necessity in order to reach performance closer to that of a human.

Compliant actuators were first introduced by Pratt an Williamson with the well-known series elastic actuator (SEA) [1]. Over the past two decades it has been investigated how these actuators can provide more suitable dynamics in unknown and dynamic environments, including humans. These actuators have various advantages such as safety, robust force control or energy efficiency. Shocks can be absorbed by the spring (mechanical filtering) and do not cause excessive wear on the transmission of the actuator improving the safety of the robots. The lower reflected inertia can improve safety when a robot is interacting with humans. Compliance can also be achieved by control [2, 3], but it presents the drawback that the bandwidth of the virtual spring is limited. Moreover, these actuators cannot store energy as there is no real compliance. A real spring can exchange energy with the environment which can reduce the power requirement. This was shown in works requiring a high burst of power (kicking, hammering, etc [4]) and cyclic tasks as the energy can be stored in the spring during negative work and then released when power generation is required [5]. In both cases, the difference, with respect

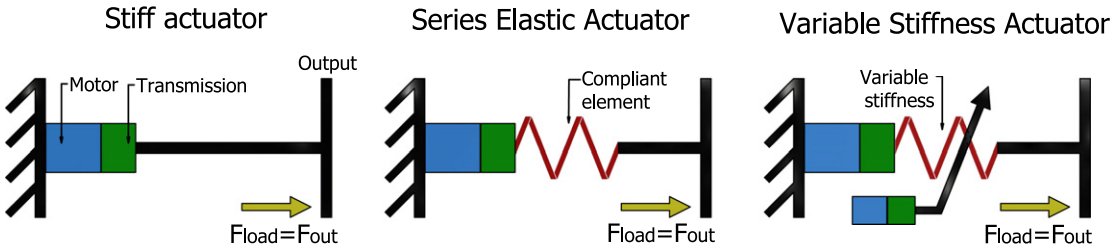

Figure 1. The linear schematics of a stiff actuator, a SEA and a VSA clarifies that the output force is proportional to the force which loads the motor $F_{load} = F_{out}$.

to a stiff actuator, is the speed profile required by the motor which can decrease the required mechanical and electrical power [6]. Further improvements also lead to the development of variable stiffness actuators (VSA) [7–9] and variable impedance actuators (VIA) where, as the name indicates, the stiffness or even the impedance can be varied. A recent review can be found in [10].

The speed profile changes for SEAs and VSAs compared to stiff actuators but the torque profile is the same. As such, the load still fully stresses the motor since they are both in series. This is depicted in figure 1 which demonstrates that the output force and the load on the motor are equal ($F_{load} = F_{out}$). Since size of a motor is proportional to the maximum continuous output torque, the used motor remains heavy and bulky [11]. Furthermore, a robotic joint typically operates at high torque and low speed, which is the opposite of the nominal operation of an electric motor. To cope with this issue, gear trains with high reduction ratios are used. Gear trains with high reductions need more stages which will decrease the efficiency as friction losses increase. Additionally, as the number of stages increases, so does the weight.

Another issue is that low speed and high torque are inefficient conditions for electric motors. The reason is that iron losses are in quadratic relation with the current, which is in turn proportional to the torque exerted by the motor. As a result, electric motors, in robotics applications, often operate significantly below their maximum efficiency.

For demanding applications such as exoskeletons or load-carrying quadrupeds, hydraulic actuators are used at a cost of low energy efficiency but excellent torque performance at high bandwidths [12]. In order to overcome torque limitations, advances in electric motors have been made to create highly dynamic motions such as the MIT Cheetah robot [13] or the strong humanoid robot Walkman [14]. Higher torque density motors have lower Joule losses and use a smaller transmission being thus more efficient. Instead of using a custom-made motor, [15] used a standard motor and applied a higher voltage than the rated one (80 V instead of 48 V) while still limiting the transient motor current, allowing to increase the maximum motor torque and velocity.

To decrease the load on the motor the spring can be placed in parallel of the motor. Such an actuator is called parallel elastic actuator (PEA). The parallel spring can decrease the load on the motor as it can provide a part of the required torque. Common examples are systems with gravity compensation [16, 17]. As the spring is always engaged, it limits the movement dexterity because the spring can also counter the desired motion. Therefore, Haeufle *et al* designed a clutchable PEA (cPEA) where the parallel spring is connected to an electrical clutch which can be disconnected from the output [18]. Au *et al* proposed another solution where they implemented a uni-directional parallel spring in their ankle prosthesis [19]. These solutions were designed for powered legs and prosthetics applications and only provide binary solutions: either the spring in parallel is engaged, with a given torque-angle profile, either it is not. These solutions may not be suited for robot applications where versatile tasks need to be performed.

The series-parallel elastic actuator (SPEA) concept addresses these issues by doing variable recruitment of parallel elastic elements. The concept is directly inspired by biological muscles. Biological muscles are composed of motor units. A motor unit consists of a motor neuron which is connected to muscle fibers through an axon. The motor neuron can activate all the motor fibers at once (ON–OFF behavior) and when activated the muscle fibers contract. Motor units differ in strength and the muscle is made of a parallel and series arrangement of them. These units are orderly recruited from the weakest to the strongest (size principle) [20]. As such few motor units are used in order to lift a light object, while more of them are recruited when heavier objects are lifted. Electric motors have higher power densities and maximum efficiency than human muscles [21]. Nonetheless, once implemented in a robotic system they cannot reach the performances that human display [22]. This means that the problem of insufficient torque and efficiency discussed in robotics applications resides in the transmission. This is important as low torque-to-weight ratio and low energy efficiency can be considered as the main factors limiting the performance of actuators driven by electric motors [23]. This motivates the use of variable recruitment to create a new

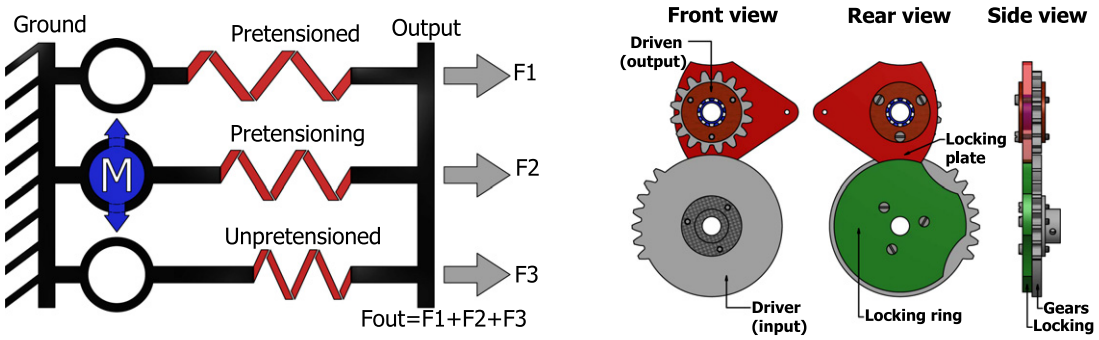

(a) The SPEA schematic shows that the output force equals the sum of the forces exerted by all springs, while the motor is only loaded by the force of the pretensioning spring.

(b) In this configuration the driver can rotate while the driven gear is locked because of the contact between the locking ring and plate. Only the driver gear can unlock the driven gear.

Figure 2. SPEA concept and intermittent mechanism used in the first prototype.

transmission between the motor and the output. This concept of variable recruitment is also used in several works with artificial muscles and electromagnetic coils [24–26]. Instead of having one muscle designed for the maximum required load, it is possible to have several muscles able to deliver the instantaneous required load (being lower than the maximum required load) for a lower pump energy consumption.

The SPEA concept is depicted in figure 2(a). A motor unit will be represented by a DC motor and a spring. There is actually only one motor which will recruit the springs one by one. When a motor unit is activated (pretensioning spring), it is in series with the motor. Once it has been fully activated (pretensioned spring) it is locked and the motor will recruit a new spring. As such only one motor is used. Furthermore, the total load F_{out} is carried by all the springs while the motor is only in series with one of them. The motor thus only carries a fraction of the load ($F_{load} = F_2$ on figure 2(a)) while the output force builds up as more springs are recruited. To variably recruit the springs, the motor has to be able to decouple itself from one spring when it is locked and couple itself to a new spring. This is realized through the use of an intermittent mechanism. An example of such a mechanism is mutilated gears depicted on figure 2(b), which were used in the SPEA proof of concept [21]. The driver gear has several teeth removed and a locking ring, while the driven gear only has an additional locking plate. When the teeth of the driver and driven gears are in contact, the gears work normally, but once the teeth of both gears are no longer in contact, the locking plate and ring will mesh each other. The locking plate and ring prevent the rotation of the driven gear, which is thus locked, but not the rotation of the driver. By placing a spring in series with the driven gear it is thus possible to tension the spring and then lock it. By placing several mutilated gears in parallel on the axis of the motor and phase shifting them, it is possible to variably recruit several springs, one by one. More details can be found in [21].

The first proof of concept showed the feasibility of lowering the motor torque requirements and increasing efficiency, but also had several drawbacks. The locking plate and ring cause friction, which is acting on the motor. Designing mutilated gears is nontrivial, leading to difficulties in the design. Furthermore, the torque of the first SPEA could only be applied in one direction, limiting the applications in which it can be used. Additionally, the total stiffness of the SPEA was constant, while it could also be of interest to have variable stiffness. In this paper, we present a novel intermittent self-closing mechanism that solves the drawbacks of the previous design. First results showing the design, a model of the locking mechanism and of the entire actuator were presented in [27]. In this paper, the design and model will be presented in more detail. The importance of the timing of actuation (phase difference) of the different layers will also be introduced. By tuning this timing, it is possible to further reduce the load on the motor for a given task. To show how this reduction of load affects the power consumption experiments using a DC motor will be presented.

The paper is organized as follows. In section 2 the novel intermittent self-closing mechanism will be introduced and it will also be explained how this mechanism was used in order to make a SPEA. Section 3 presents the design of one layer and the self-closing mechanism used. This will be followed by a model of the locking and the output torque as well as the torque loading the motor. In section 4 the setup with all the layers will be considered and the model will thus be extended to the SPEA. In order to demonstrate the lower energy consumption experiments with measurements of the electrical consumption of a motor with the SPEA are given in section 5. Section 6 will

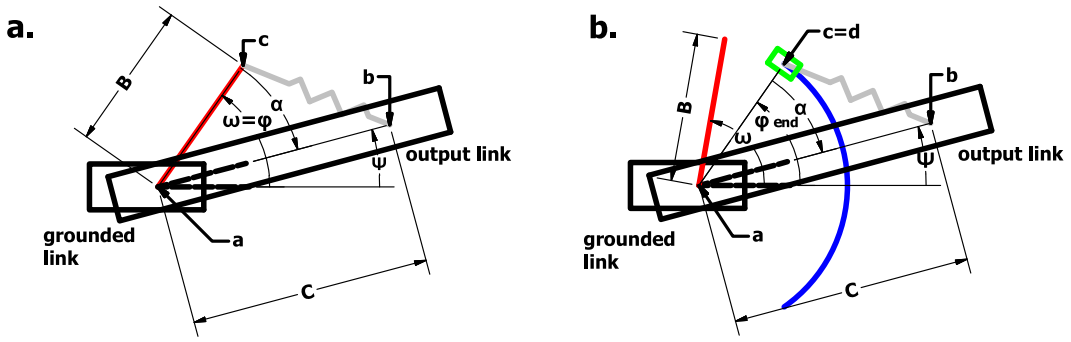

(a) Schematic and nomenclature of the standard MACCEPA.

(b) Schematic and nomenclature of the intermittent MACCEPA with guide (blue) and tensioner (green). Here the motor arm (red) is disconnected from the spring as $\omega > |\varphi_{end}|$.

Figure 3. Standard and intermittent versions of the MACCEPA (reproduced with permission from [27], copyright 2014).

conclude the paper and gives some perspective for future work on the SPEA.

2. New concept of the SPEA

In order to have a SPEA with bi-directional torque and variable stiffness, the design of an existing VSA having both these properties was adapted. The actuator used is the mechanically adjustable compliant and controllable equilibrium position actuator (MACCEPA) [7]. The design was modified such that the motor can be decoupled from the springs and lock them, but also so that different layers of this modified VSA can be combined together and, intermittently, actuated by only one motor. This will be detailed in section 2.1. Then it will be explained in section 2.2 how the different layers of this intermittent MACCEPA act together when used for a SPEA.

2.1. Intermittent MACCEPA

The MACCEPA is a VSA with a very simple design. The schematic of the standard MACCEPA is shown on figure 3(a). The actuator consists of 3 bodies (grounded link, motor arm and output link) rotating around the point a. The grounded link is supposed to be fixed. The motor arm, of length B (in red), changes the equilibrium position of the actuator (φ), and its position relative to the grounded link is given by ω (in this case $\omega = \varphi$). There is a spring, of constant stiffness k, placed between the motor arm and the output link. It is placed between the points c and b where c belongs to the motor arm and b belongs to the output link (the length ab is C). The angle $\angle bac$ (α) is the deviation from the equilibrium angle. When the motor arm and the output link are not aligned ($\alpha \neq 0$) the spring is extended. This results in a spring force which will create a torque that tends to align both bodies unless an external torque is applied. The position of the output link with respect to the grounded link is given by $\Psi = \varphi + \alpha$.

It can be shown [7] that the external torque applied to the motor arm and output link is given by [27]:

$$T = kBC \sin\alpha \left(1 + \frac{P - C + B + F_0/k}{\sqrt{B^2 + C^2 - 2BC\cos\alpha}}\right) \quad (1)$$

P is the pretension of the spring which can be controlled by an additional motor. One can notice that with pretension there is a spring force when the motor arm and the output link are aligned, but there is no torque. By changing the pretension of the spring the stiffness of the actuator ($\mathrm{d}T/\mathrm{d}\alpha$) can be modified. One can notice that the torque is not dependent of the equilibrium position and thus both motors are able to control the equilibrium position (through ω) and the stiffness (through P) of the actuator independently. When using extension springs an initial tension (F_0), acting as an additional pretension, has to be accounted for when significant in comparison to the total spring force.

In order to use the MACCEPA for a SPEA it is required to be able to decouple the motor arm and the spring. The mechanism used to achieve this is inspired from self-closing mechanisms. Self-closing mechanisms are generally used in drawers [28, 29] and allow the drawer to close itself, via a spring (sometimes combined with a damper), when slightly opened. When fully opened the spring is decoupled from the drawer. As such the drawer remains open without having to constantly apply a force on it. The mechanism developed is depicted on figure 3(b). There are two additional elements to the standard MACCEPA: the guide, in blue, and the tensioner, in green. The tensioner is directly connected to the spring and moves along the guide which is fixed on the grounded link. As shown in figure 3(b), when the amplitude of the motor angle $|\omega|$ exceeds φ_{end} it is decoupled from the tensioner and thus from the spring. The tensioner is locked when it reaches the end of the guide (denoted by the point d)

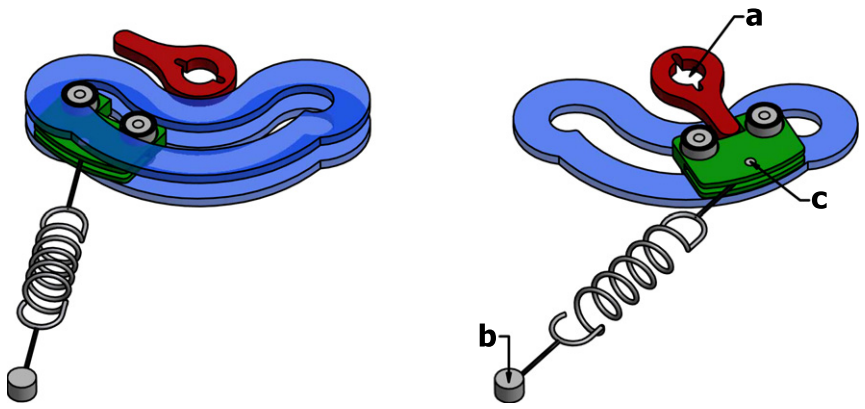

(a) The motor arm (in red) is decoupled from the spring. The tensioner (in green) is at the end of the guides (in blue). The shape of the guides is designed such that when the motor arm pushes the tensioner towards the end of the guide it will automatically lock itself and remains locked after the arm is decoupled from the tensioner. The tensioner is in contact with the guide through 4 legs which are bearings in order to reduce the friction.

(b) The arm is pushing the tensioner which is moving inside the guide (one of the two guides is not represented for clarity). In this configuration the motor arm is in series with the spring. The tensioner has a slot accommodating the motor arm. This slot, as well as the end of the guide, are designed such that the motor arm is able to leave the tensioner when $|\omega| > \varphi_{end}$ but also that it can, when going back, unlock the tensioner.

Figure 4. Intermittent MACCEPA when the tensioner and the motor arm are (de-)coupled (reproduced with permission from [27], copyright 2014).

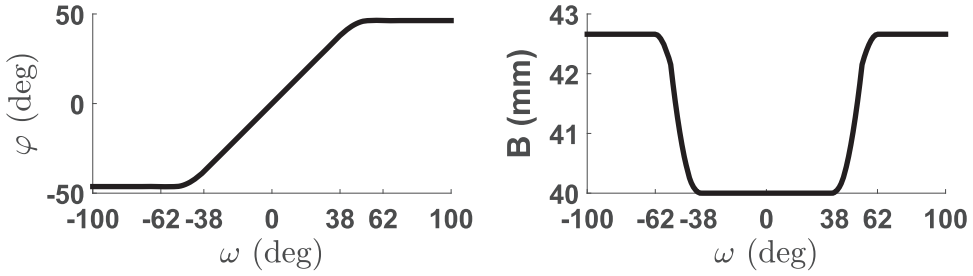

Figure 5. For $|\omega| < 38°$ the relationship between φ and ω is linear as the tensioner is simply rotating around the point a. For the same reason B is constant (and is equal to 40 mm). For $38° \leqslant |\omega| \leqslant 62°$ the tensioner is reaching the end of the guide and φ and B behave nonlinearly with ω. For $|\omega| > 62°$ the motor arm and the tensioner are decoupled and as such B and φ are constant ($B = 42.66$ mm and $\varphi(\omega = -62°) = -\varphi_{\text{end}} = -46°$).

and can only be unlocked when the motor arm goes back. As such the relationship between the equilibrium angle φ and the motor angle ω is defined as follows [27]:

$$\varphi(\omega) = \begin{cases} -\varphi_{\text{end}} & \omega < -\varphi_{\text{end}} \\ \omega & \text{if } -\varphi_{\text{end}} \leqslant \omega \leqslant \varphi_{\text{end}} \\ \varphi_{\text{end}} & \varphi_{\text{end}} < \omega \end{cases}. \tag{2}$$

When $|\omega| < \varphi_{\text{end}}$ the motor arm (and thus the motor setting the equilibrium position) is connected in series with the spring (and the output link) while the spring is decoupled from the motor when $|\omega| > \varphi_{\text{end}}$. As such the intermittence is introduced. Moreover, this locking mechanism does not create any friction on the motor, contrary to mutilated gears. It is also important to notice that the range of the equilibrium angle is now physically limited to $[-\varphi_{\text{end}}; \varphi_{\text{end}}]$.

Contrary to what is indicated by figure 3(b), the guide is not completely circular. It is required, when the tensioner reaches the end of the guides (hence $\varphi = \pm\varphi_{\text{end}}$), that the tensioner remains at this position (locked) and that the motor arm is no more coupled to it. The real shape of the guide and the tensioner is therefore depicted in figure 4.

Because of the shape of the extremities of the guide, the relationship between the position of the motor arm (ω) and the equilibrium position (φ) is more complicated than the one presented in equation (2). Similarly, the length B, which is the distance between points a and c, is no longer constant ($B = B(\omega)$) simply because the point c now belongs to the tensioner (while it belonged to the motor arm in the standard MACCEPA). The influence of the end of the guide on the intermittent MACCEPA will be detailed in section 3, but figure 5 already displays the dependence of B and φ as a function of ω for the actual setup.

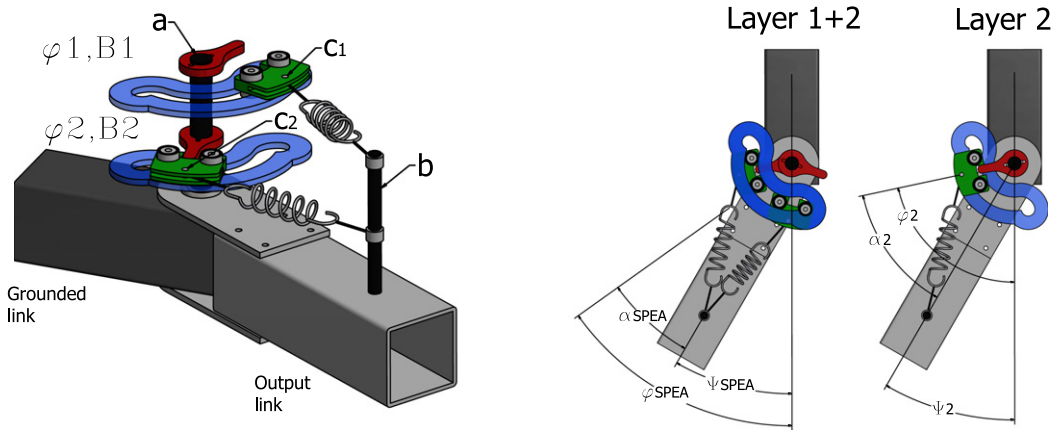

(a) The two layers have two common axes: the axis a around which the motor arms rotate and the axis b, which connects the two layers to the output link. Thus the points a and b are common to every layer, but the points c are not aligned (see c_1 and c_2).

(b) Each layer has its own angles Ψ_i, φ_i and α_i. The SPEA also has its own angles $\Psi_{SPEA}, \varphi_{SPEA}$ and α_{SPEA}. Only $\Psi_i = \Psi_{SPEA}$ for every i while it is not the case for the other variables (φ_i, α_i and B_i).

Figure 6. SPEA with two layers.

It can be noticed that the same modifications can be done to other VSAs to build an SPEA. AWAS [30], for example, if the mechanism varying the stiffness is not included, has a spring placed between the link setting the equilibrium position and the output which is similar to the MACCEPA. In this case a guide and tensioner can also be used to convert this VSA into a self-closing mechanism. As self-closing mechanisms are used for drawers they normally perform a linear motion and thus it could also be adapted to prismatic compliant actuators.

2.2. Stacking

By using several layers and actuating them intermittently, it is possible to reduce the load on the motor. The reason is that the total torque will be distributed amongst the different layers, while the motor is in series with only one (or possibly several of them). Here, the layers will simply be stacked on top of each other. A SPEA with two layers is depicted in figure 6. The motor changing the equilibrium position of the SPEA actuates the axis a (motor axis). The motor arms of every layer are fixed on this axis and are phase shifted from each other. As the motor axis rotates, the motor arms will successively unlock the tensioners and lock them on the opposite side.

On figure 6(a) the spring of the first layer is not connected to its motor arm, while the tensioner of the second layer is actuated by the second motor arm. As such the first spring acts in parallel while the second spring is in series with the motor. The contribution provided by the first spring can lower the torque that has to be provided by the motor. The difference to a PEA+SEA is that the torque profile provided by the first spring can be changed if it is locked on the other side. It could be said that it is a PEA+SEA where the equilibrium position of the parallel spring can have two discrete values. Compared to gravity compensation systems which can only cancel one specific load, the SPEA has the advantage of canceling variable loads. As it will be shown in section 4 the load on the motor can be decreased by a factor equal to the number of layers, showing the potential of this actuator.

There are only two additional variables when going from the intermittent MACCEPA to the SPEA: the number of layers (n) and the phase difference between the motor arms of each layer ($\xi\Delta\omega$). $\Delta\omega$ is the angle the motor has traveled from the moment a tensioner has been unlocked from one side and locked to the other side by a motor arm. This angle can roughly be approximated by $2\varphi_{\text{end}}$ ($\Delta\omega = 2 * 62^\circ$ and $2\varphi_{\text{end}} = 2 * 46^\circ$ on figure 5). $\xi \in [0; 1]$ is the shifting parameter and will define how many layers are actuated simultaneously. The phase difference between two arms is depicted in figure 7(a) and the effect of two phase differences on the actuation sequence ($\text{Act}_i(\omega)$) of four layers is given on figure 7(b). One can see that for $\xi = 1$ the layers are actuated one by one while there are several overlapping of the actuation of the different layers for $\xi = 0.6$. The importance of this parameter will be discussed in section 4.

The main limitation of this implementation is the maximum number of layers that can be placed for a given range of equilibrium angles. The maximum angle that a motor arm can travel is limited to $2\pi + \Delta\omega$. Thus the angle to move the tensioner from one side to the other ($\Delta\omega$) plus a complete turn after which the motor arm hit back the tensioner locked (if one neglects its dimension). On the other hand the maximum motor angle traveled by the motor for the whole actuation of the SPEA is equal to $(n-1)\xi\Delta\omega + \Delta\omega$. $(n-1)\xi\Delta\omega$ is the total angle traveled from the first arm until the last arm starts to

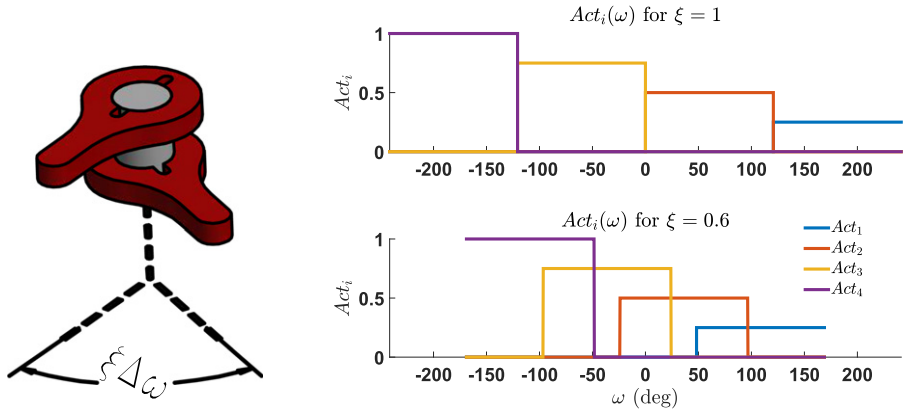

(a) The angle between 2 consecutive motor arms is $\xi\Delta\omega$.

(b) $Act_i(\omega)$ is larger than one when a layer is actuated and equal to zero otherwise. One can notice that for $\xi = 0.6$ layer 3 and 4 are being actuated simultaneously at $\omega = -60°$ while all layers are actuated separately for $\xi = 1$.

Figure 7. Phase difference between the arms and effect on the actuation.

Table 1. MACCEPA parameters of the SPEA.

$T_{o,\max}$	φ_{end}	$\Psi_{\max}$	n	k	B_{MACCEPA}	C	$P_{\max}$
3 Nm	45°	40°	4	0.51 N mm^{-1}	40 mm	130 mm	15 mm

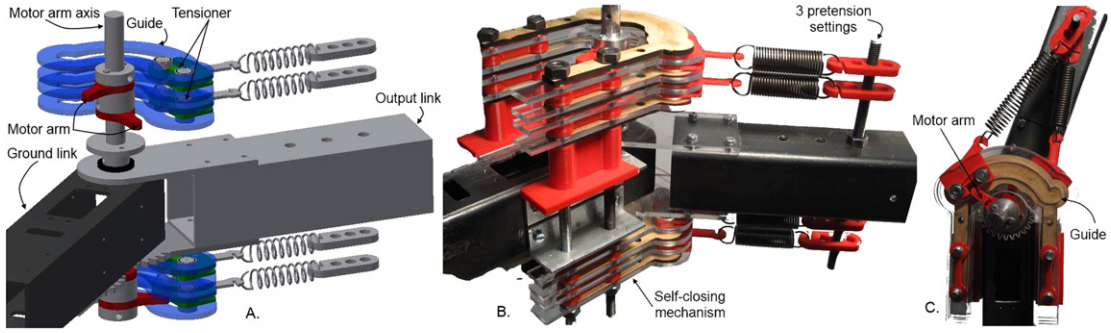

Figure 8. A and B: 3D drawing and a picture of the MACCEPA-based SPEA with four layers. B: close-up on the tensioner and the guide. C: top view of the actuator. On figure B one can see that the connections between the springs and the output link have three holes in it, thus allowing three different pretension settings ($P = 5, 10$ or 15 mm) (reproduced with permission from [27], copyright 2014).

unlock its tensioner and $\Delta\omega$ is the travel distance to lock this tensioner to the other side. The first requirement for the SPEA to work is to ensure that the first motor arm does not hit its tensioner during the actuation of the SPEA (hence having $(n-1)\xi\Delta\omega + \Delta\omega < 2\pi + \Delta\omega$). By using the approximation $\Delta\omega \approx 2\varphi_{\text{end}}$ one can compute the maximum number of layers for a given range of equilibrium angles (this is an over-estimation as $2\varphi_{\text{end}} < \Delta\omega$):

$$n_{\max} = 1 + \left\lfloor \frac{\pi}{\xi\varphi_{\text{end}}} \right\rfloor. \tag{3}$$

The second requirement for the SPEA to work is that the tensioners should remain locked once they reach the end of the guides. With $[-\Psi_{\max}; \Psi_{\max}]$ defining the working range of the actuator, the locking mechanism has to be designed such that all the tensioners remain locked for $\Psi \in [-\Psi_{\max}; \Psi_{\max}]$. It will be detailed in section 3.2 how the locking provided by the guide can be modeled.

By defining $\Psi_{\max}$, φ_{end} and the maximum output torque $T_{o,\max}$ most of the design parameters of the actuator can be chosen. The maximum torque delivered by each layer is assumed to be equal to $T_{o,\max}/n$. Starting with a requirement on the maximum size (e.g a maximum value for C) of the actuator and a maximum deviation angle $\alpha_{\max} \approx \Psi_{\max} + \varphi_{\text{end}}$ proper values for B, k, $P_{\max}$ (maximum pretension) can be selected. In order to show the influence of ξ the test

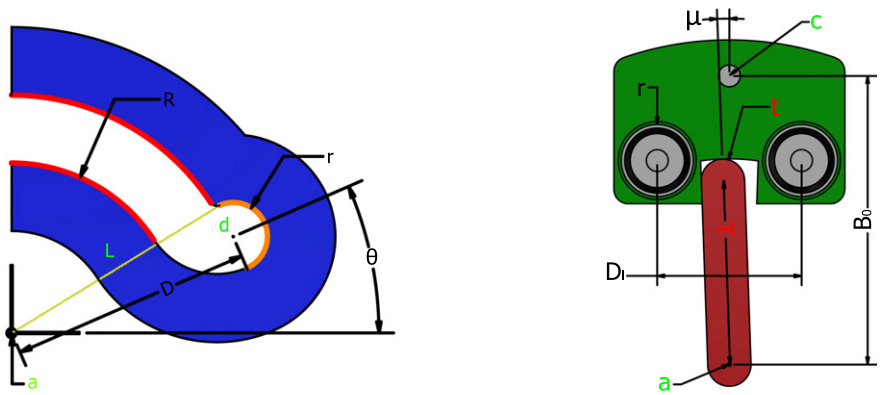

(a) The guide (inner part which is in contact with the legs of the tensioner) is composed of 5 circular arcs: 2 main arcs (in red) of radius R, $R + 2r$ and of center a, an arc of radius r and center d (in orange) which is the end of the guide and 2 arcs connect the 3 previous arcs together. The neighboring arcs are all tangent to each other. The length between a and d is denoted by D and the angle between the segment ad and the horizontal axis is θ. A segment (L) connecting the point a to the arc of circle of radius r is tangent to this arc.

(b) The tensioner has 2 legs whose distance from each other is D_l. The legs have a radius r (already defined for the guide). The guide has also a slot accommodating the motor arm. The motor arm has a length T and the head is an arc of radius t. B_0 is the distance between the point a and c. μ is the angle between the motor arm and the segment ac when the motor arm is resting against the tensioner.

Figure 9. Design parameters of the guide, tensioner and motor arm (reproduced with permission from [27], copyright 2014).

setup was built using $\xi = 1$ as it is always possible to use a smaller phase difference between the arms afterwards. The different parameters of the setup are given in table 1. The test setup built is depicted in figure 8.

3. One layer model

The characteristics of the intermittent MACCEPA are mainly defined by the design of the guide. The different design parameters for the guide, tensioner and motor arm is given in section 3.1.

The main goal of the guide is to ensure that the tensioner remains locked when it reaches the end of the guide and that the motor arm leaves the slot inside of which it was accommodated. A model of the locking provided by the guide is presented in section 3.2. As mentioned in section 2.1, the shape of the guide will lead to a nonlinear relationship between the equilibrium position φ and the length B as a function of the motor angle ω, which is not the case for the standard MACCEPA. This will be further detailed in section 3.3 and an explanation of figure 5 will also be provided.

For the standard MACCEPA, the torque provided by the motor setting the equilibrium position and the torque provided at the output are equal, but because of the reaction forces between the guide and the tensioner, this is no longer the case for the intermittent MACCEPA and this will be discussed in section 3.4.

The design of the guide, tensioner and motor arm as the model of the locking and load torque were already presented in [27] but the reader is invited to pay attention to the model presented in this paper as the nomenclature has changed.

3.1. Design of the guide, motor arm and tensioner

The main design parameters of the guide, as well as the tensioner and the motor arm are given in figure 9.

What follows is an explanation regarding the selection of the design parameters and how they are related to the parameters of the standard MACCEPA that were defined in section 2.2:

- Tensioner:
  - B_0 gives is the value of $B(\omega = 0)$ (B when the tensioner is in the middle of the guide). Although the value of $B(\omega)$ is not constant, it is close to B_0 (see figure 5 with $B_0 = 40$ mm) and thus B_0 can be used as an approximation of B.
  - μ leads to a certain backlash which is necessary to ensure that the motor arm can engage and disengage the tensioner when it is at the end of the guide.
- Guide:
  - $R + 2r$ should be selected close of B_0.
  - $(\pi/2 - \theta)$ roughly gives the maximum equilibrium angle (φ_{end}) that is desired, but this angle does not change the shape of the end of the guide. It only changes the length of the two main arcs of the guide depicted on figure 9(a).
  - D will change the complete shape of the guide. This variable should be adapted such that sufficient locking is provided. By taking this value equal to $R + 2r$ the end of the guide and the main circular arcs are directly in contact

Table 2. Design parameters of the SPEA.

R	D	r	θ	D_l	B_0	μ	T	t
25 mm	35.5 mm	5 mm	23.5°	20 mm	40 mm	2°	24.5 mm	3 mm

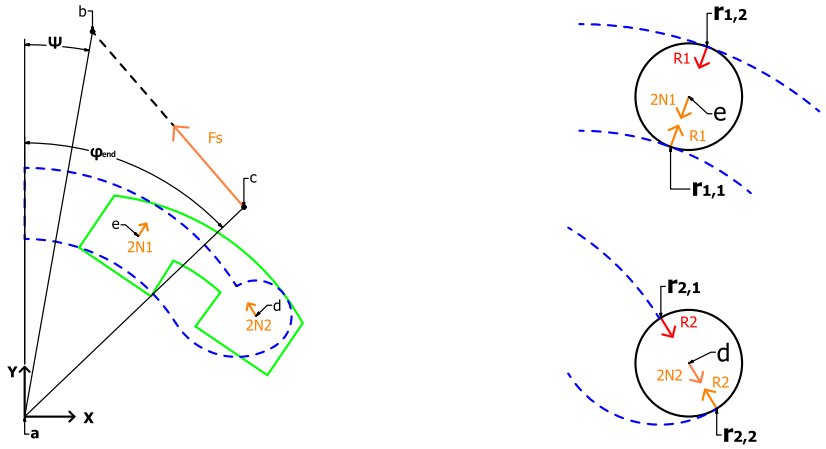

(a) Free body diagram of the tensioner. There are 3 forces acting on the tensioner: the spring force F_s at point c, the reaction force of the fixation of the first leg of the tensioner (N_1) acting at point e and the reaction force of the second leg of the tensioner (N_2) acting at point d. There is a factor 2 in front of the reaction forces because there are four legs in total (two on each side).

(b) Free body diagram of the legs of the tensioner. There are 2 forces acting on the legs: the reaction forces between the legs and the tensioner defined on Fig. 10a and the reaction forces between the legs and the guides R_1 and R_2. Depending on the direction of the spring force the legs of the tensioner can be in contact with the guide at different points: either $r_{1,1}$ or $r_{1,2}$ for the first leg and either $r_{2,1}$ or $r_{2,2}$ for the second. Depending on the point of contact the sense of the reaction forces will change (see red and orange arrows) but both forces have the same direction.

Figure 10. Free body diagram of the tensioner, without its legs, and free body diagram of the legs of the tensioner.

(one arc disappears) which gives a rough edge. Thus $D > R + 2r$, but as D increases, the difference between the maximum value of $B(\omega)$ and B_0 increases and $\varphi(\omega)$ deviates more from equation (2) which should be avoided.

- Motor arm:
  - The radius t and length T should be selected such that the motor arm can withstand the forces and torques acting on it and such that it correctly actuates the tensioner.

The value of the different parameters used to design the guide, tensioner and motor arm are given in table 2. For reproducibility of the results, a .stp file containing the CAD drawings of the guide, tensioner and motor arm has been provided as supplementary material (stacks.iop.org/bb/11/016005/mmedia)

3.2. Locking region

Once the tensioner reaches the end of the guide, it should remain locked in this position for a certain range of output angles Ψ (thus for $\Psi \in [-\Psi_{max}; \Psi_{max}]$). Figure 10(a) gives the free body diagram of the tensioner without its legs, while figure 10(b) gives the free body diagram of the legs of the tensioner. For simplicity only the forces in the plane are considered and gravity is neglected (the spring force being two orders of magnitude higher). Furthermore friction will also be neglected which is a conservative approach since friction should improve the locking.

The balance of the forces acting on the tensioner is expressed with respect to the grounded link (in the xy frame depicted in figure 10(a)) and torques are computed around the point e. The balance of the forces on the legs can be expressed by using the amplitudes of the forces directly (since the two forces are aligned there is no torque balance) [27]:

$$\begin{cases} F_{s,x} + 2N_{1,x} + 2N_{2,x} = 0 \\ F_{s,y} + 2N_{1,y} + 2N_{2,y} = 0 \\ \overrightarrow{ed} \times 2\overrightarrow{N_2} + \overrightarrow{ec} \times \overrightarrow{F_s} = 0 \end{cases}$$
$$\begin{cases} R_1 \pm 2N_1 = 0 \\ R_2 \pm 2N_2 = 0. \end{cases} \quad (4)$$

The geometry of the guide, as the geometry of the tensioner, are included in equation (4). For example, the orientation of the reaction forces N_1 and N_2

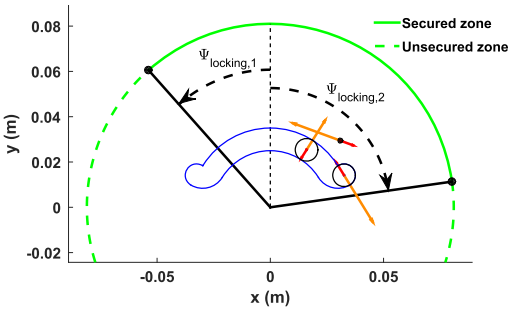

(a) Balance of the forces on the tension when in equilibrium (orange and red arrows). The 2 angles $\Psi_{locking}$ define the zones inside of which the locking is secured/unsecured.

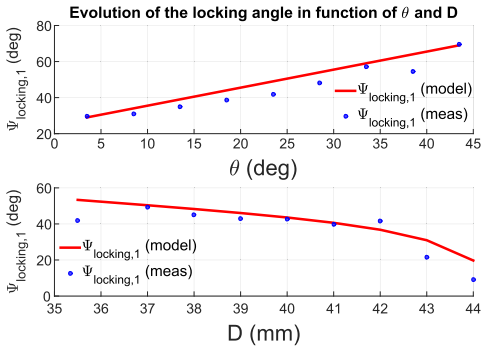

(b) Experiments of the locking region of 18 guides with different design variables θ and D approximate the modeled locking region (R=25mm, r=5mm, D_l=20mm, B_0=40mm, $\mu = 2°$) [27].

Figure 11. Representation of the safe/unsafe zones and experimental validation of Ψ_{locking}.

depends on the design of the guide. The force of the spring F_s is dependent of the output angle Ψ [27]:

$$\begin{cases} F_{s,x} &= F_s(\overrightarrow{1_{F_s}} \cdot \overrightarrow{1_x}) = F_s(x_b(\Psi) - x_c(\varphi_{\text{end}}))/l \\ F_{s,y} &= F_s(\overrightarrow{1_{F_s}} \cdot \overrightarrow{1_y}) = F_s(y_b(\Psi) - y_c(\varphi_{\text{end}}))/l \end{cases} \quad (5)$$

$l = \sqrt{(x_b(\Psi) - x_c(\varphi_{\text{end}}))^2 + (y_b(\Psi) - y_c(\varphi_{\text{end}}))^2}$ and F_s is the amplitude of the force of the spring. There are five unknowns in equation (4): N_1, R_1, N_2, R_2 and Ψ.

As mentioned previously there are different possibilities regarding the points of contact between the guide and the legs of the tensioner. The points of contact between the legs of the tensioner and the guide can be found by solving the left side of equation (4). Indeed, the reactions forces R_1 and R_2 always need to be positive (this is how the different cases can be differentiated). If the numerical value of N_1 is positive but the value of N_2 is negative, one knows that the points of contact are $r_{1,1}$ and $r_{2,2}$ (this explains the $\pm$ sign in equation (4)).

Solving equation (4) will give 2 values for Ψ, N_1 and N_2 (this is due to the trigonometric relationships present in equations (4) and (5)). Thus 2 angles Ψ are found (called Ψ_{locking}) and these angles correspond to the cases where the tensioner is in equilibrium. If $\Psi \neq \Psi_{\text{locking}}$ then the balance of the forces and torques is nonzero, meaning that there is an acceleration/rotation and thus a movement of the tensioner (unlocking). Due to the shape of the guide, the tensioner can only move towards the left. Moving to the right is impossible because the end of guide acts as an obstacle. This means that the angles Ψ_{locking} define 2 zones where the locking is secured/unsecured. This is depicted on figure 11(a).

The model of the locking was experimentally validated by using several guides with different design parameters and measuring the output angles at which the tensioner unlocked. The results are shown on figure 11(b). Only $\Psi_{\text{locking},1}$ could be measured because $\Psi_{\text{locking},2}$ could not be reached mechanically with the setup for most of the guides tested. Nine guides with different values for D ranging from 34.5 mm to 44 mm with a fixed value of $\theta = 23.5°$ and nine other guides with different θ ranging from 3.5°–43.5° with a fixed value of $D = 35.5$ mm were used. The average of five values was taken and the standard deviation is smaller than the marker size.

One can observe that the zone where the locking is secured just shifts as θ increases. This is expected because, as mentioned in section 3.1, the angle θ does not influence the end of the guide but changes its position relative to the xy frame. If one considers the configuration of forces at which the tensioner unlocks for an angle θ_1, the configuration of forces will be exactly the same for an angle θ_2 except that this configuration has rotated of an angle $\theta_1 - \theta_2$ around the point a (as the end of the guide itself has simply rotated of the same angle). This will translate into a linear variation of Ψ_{locking} with θ.

Since D changes the end of the guide, its influence will modify the safe and unsafe zones. Increasing D will result in a reduction of the safe zone. Indeed, as D increases, the tensioner unlocks for angles closer to $\Psi = 0°$, while Ψ_{locking} should be higher than $\Psi_{\text{max}} = 40°$ (see table 1).

Furthermore it can be observed that the model and the measurements are in good agreement showing that the model proposed can be used in order to design a guide providing a safe locking.

3.3. Equilibrium position and lever arm *B*

As mentioned in section 2.1, the relationship between φ and ω is nonlinear and will depend on the design of

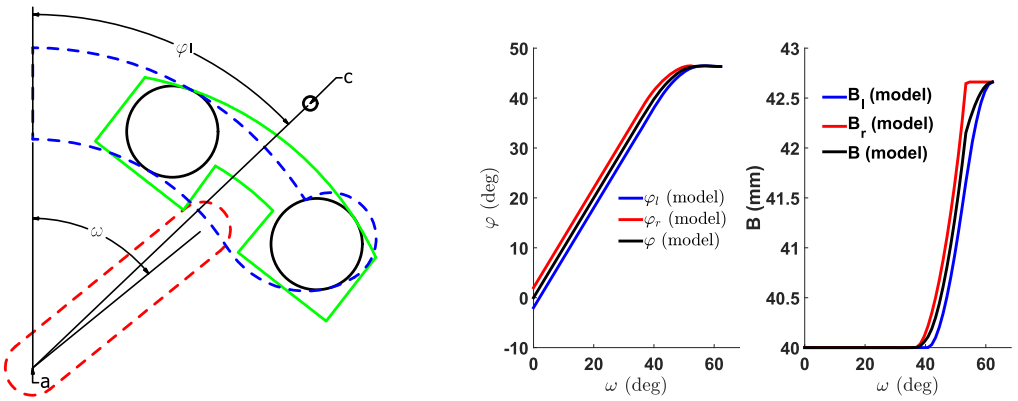

(a) Motor arm in contact with the left wall of the tensioner. The equilibrium position is denoted $\varphi_l(\omega)$.

(b) φ_l and φ_r in function of ω for the actual setup. φ is simply the mean value of φ_l and φ_r. $B, B_{l,r}$ are defined in a similar way as the angles φ, φ_l and φ_r.

Figure 12. Kinematic model of the tensioner.

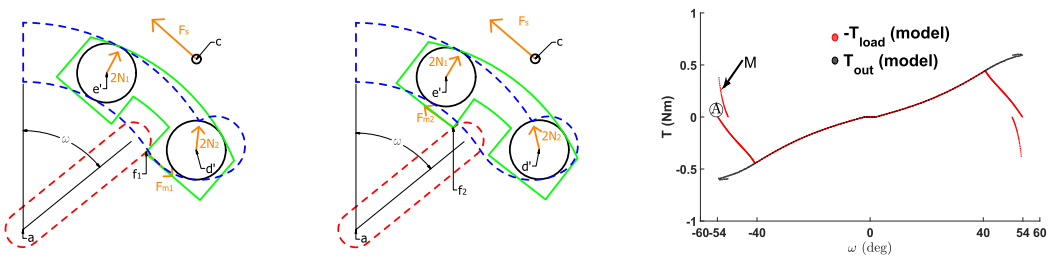

(a) Force balance on the tensioner, f_1 being the point of contact between the motor arm and the tensioner.

(b) Force balance on the tensioner, f_2 being the point of contact between the motor arm and the tensioner.

(c) Expected load (red dots) and output (black dots) torque in function of ω for a blocked output simulation.

Figure 13. Model of the load torque.

the guide, tensioner and motor arm. The relationship is also not bijective. On figure 12(a) the arm is pushing on the left edge of the tensioner, but it could also be pushing on the right edge depending on the force of the spring and the curvature of the guide. Thus for a given motor angle ω, the tensioner has two possible positions (thus there are two possible values of φ and B for ω).

The possible equilibrium positions and lever arms for a given ω are denoted by $\varphi_{l,r}$ and $B_{l,r}$.

For simplicity, a uniquely defined relationship between φ and ω should be used. This is simply done by taking the mean value between φ_l and φ_r: $\varphi = (\varphi_r + \varphi_l)/2$. The same is done for $B(\omega)$ and both relationships are shown on figure 12(b).

For $|\omega| < 38°$ the difference between φ_m and $\varphi_{l,r}$ is constant and equal to μ which is the backlash of the tensioner when it is rotating around the point a. B is constant for $|\omega| < 38°$ and equal to B_0 for the same reason (the point c is rotating around a and the distance between the 2 points was defined as B_0 in section 3.1).

Equation (2) can now be written as:

$$\varphi(\omega) = \begin{cases} -\varphi_{\text{end}} & \omega < \omega^- = -\Delta\omega/2 \\ f_\varphi(\omega) \quad \text{if} \quad \omega^- \leqslant \omega \leqslant \omega^+ & \\ \varphi_{\text{end}} & \omega > \omega^+ = \Delta\omega/2 \end{cases} \tag{6}$$

$f_\varphi(\omega)$ is the function that defines the equilibrium position when the tensioner is actuated by the motor arm. The angle at which the tensioner starts to be actuated (or is locked) on the left side is ω^- (ω^+ is used for the right side).

3.4. Output and load torques

In case of the standard MACCEPA, the torque loading the motor (T_{load}) setting the equilibrium position and the torque at the output (T_{out}) are equal because the motor arm is connected to the output through the spring (thus both bodies are connected in series). In the case of the intermittent MACCEPA, the motor arm is actually pushing the tensioner, connected to the output through the spring, which is sliding inside of

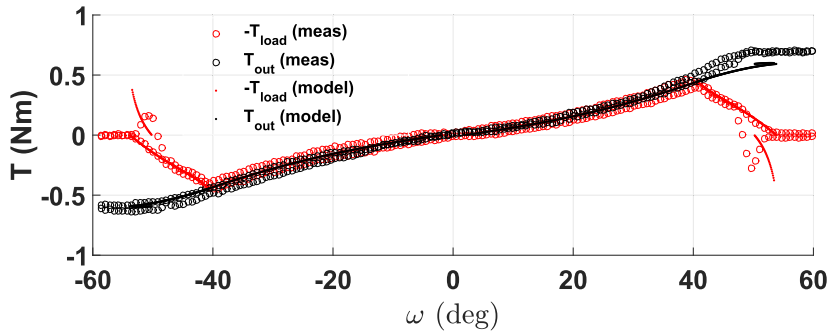

Figure 14. The expected load and output torques match the model although the unlocking occurs for a lower angle ω than predicted, probably because of inaccuracies in the construction of the guide, tensioner and motor arm (reproduced with permission from [27], copyright 2014).

the guide. This makes a difference since there are also reaction forces between the tensioner and the guide.

A kinetostatic model will be developed to show how the load and output torque differ. The assumptions are the same as for the model of the locking. The forces acting on the tensioner, when it is actuated by the motor arm, are depicted on figure 13(a). One additional force is present in comparison to the model of the locking: the force developed by the motor arm F_{mj} ($j = 1, 2$). As discussed in section 3.3, for a given angle ω there can be two possible configurations of the tensioner. Only one of the two configurations is correct. By comparing figures 13(a) and (b) it can be intuitively found that it is the configuration of figure 13(a) which is the correct one. The simplest way to determine the correct configuration is to solve both problems and determine the sign of F_{mj}. If $F_{mj} < 0$, this means that the arm is not pushing the tensioner but pulling it, which is impossible. Hence the considered configuration is impossible.

The balance of the forces and torques (this time around the point a) is given by [27]:

$$\begin{cases} F_{m,x} + F_{s,x} + 2N_{1,x} + 2N_{2,x} = 0 \\ F_{m,y} + F_{s,y} + 2N_{1,y} + 2N_{2,y} = 0 \\ \overrightarrow{ae'} \times 2\overrightarrow{N_1} + \overrightarrow{ad'} \times 2\overrightarrow{N_2} + \overrightarrow{af_j} \times \overrightarrow{F_{mj}} \cdot \\ \quad + \overrightarrow{ac} \times \overrightarrow{F_s} = \overrightarrow{0} \end{cases} \quad (7)$$

The load torque on the motor (arm) is equal to $-\overrightarrow{af_j} \times \overrightarrow{F_{mj}}$ and one can notice that $\overrightarrow{ac} \times \overrightarrow{F_s}$ is equal to equation (1). N_1 and N_2 are the radial forces acting on the bearings (as computed for the locking) and they can be used to check if the bearings are correctly sized by comparing these forces to their maximum static load. When the legs of the tensioner are in contact with the main circular arcs, the normal forces are parallel to the vectors $\overrightarrow{ae'}$ and/or $\overrightarrow{ad'}$. This is the case in figure 13(a) where $\overrightarrow{ae'} \times \overrightarrow{N_1} = \overrightarrow{0}$ (but $\overrightarrow{ad'} \times \overrightarrow{N_2} \neq \overrightarrow{0}$). In the case where both reaction forces do not produce any torque it follows that:

$$\overrightarrow{af_j} \times \overrightarrow{F_{mj}} + \overrightarrow{ac} \times \overrightarrow{F_s} = \overrightarrow{0}. \quad (8)$$

The load torque is then equal to the output torque and the intermittent MACCEPA behaves as the standard MACCEPA.

To show the difference between the load and output torques, a blocked output simulation, based on the developed model, was performed. The ground and output links are aligned and the output link is blocked (hence $\Psi = 0°$). The motor angle then goes from $-\Delta\omega/2$ to $\Delta\omega/2$ (thus the tensioner is moved from one end of the guide to the other). The results from the simulation are given in figure 13(c). For $|\omega| < 40°$ the output and load torques are equal, because the reaction forces of the bearings give no torques. For $|\omega| > 40°$ the load torque starts to decrease, while the output torque increases. The output torque continues to increase because the extension and the lever arm of the spring increase. However the load decreases simply because the reaction forces (hence the structure) take over a part of the load. At $\omega \approx 54°$ the load torque is zero (point A). If the motor arm pushes the tensioner further, it will directly move towards the end of the guide (locking). When the motor arm tries to unlock the tensioner, the torque will be given by the curve M. The torque is now negative and represents the locking torque that needs to be overcome to unlock the tensioner. Now the reaction forces try to push back the tensioner in the lock position if it is moved away from it. Once this torque increases to zero (again for $\omega \approx 54°$) the tensioner will be unlocked. This explains why the load torque is not continuous and can have different values for the same ω.

The load and output torques were measured on a test setup to validate the model. The results are depicted on figure 14. A Futek force sensor was placed on the output link (at a distance of 45 mm from the point a) to measure the torque at the output. A torque sensor ETH messtechnik DRBK was placed on the motor axis to measure the load torque. The measured load torque is slightly lower than the output torque which may be due to imprecision in the measurements. Nonetheless,

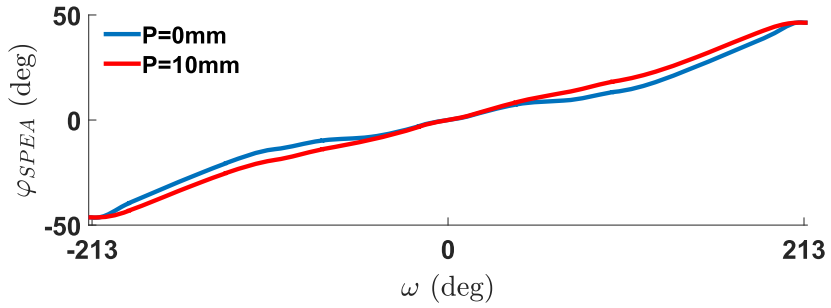

Figure 15. Modeled equilibrium position of the SPEA φ_{SPEA} in function of the motor angle ω for two pretension settings. $\varphi_{\text{SPEA}} = \pm\varphi_{\text{end}}$ (four tensioners locked on the left/right) and $\varphi_{\text{SPEA}} = 0$ (two tensioners locked on the left and two locked on the right) are independent of the pretension setting.

the model allows to accurately predict the behavior of the mechanism.

4. Stacking of several units

In this section the effect of stacking several layers on top of each other will be studied. The previous study on the behavior of one layer in section 3 can be applied here with few changes. First, the denotation for one layer is extended to several layers, using an index i to differentiate between them. Next, the equilibrium position of each layer will now be written as:

$$\begin{aligned}
\varphi_i(\omega) &= \begin{cases} -\varphi_{\text{end}} & \omega < \bar{\omega_i} \\ f_\varphi(\omega_i^*) & \bar{\omega_i} \leqslant \omega \leqslant \omega_i^+ \\ \varphi_{\text{end}} & \omega_i^+ < \omega \end{cases} \\
\bar{\omega_i} &= \Delta\omega\left(\xi\left(\mathrm{i} - \frac{n+1}{2}\right) - \frac{1}{2}\right) \\
\omega_i^+ &= \Delta\omega\left(\xi\left(\mathrm{i} - \frac{n+1}{2}\right) + \frac{1}{2}\right) \\
\omega_i^*(\omega) &= \omega - \xi\Delta\omega\left(\mathrm{i} - \frac{n+1}{2}\right)
\end{aligned} \tag{9}$$

$\bar{\omega_i}$ and ω_i^+ are defined, similarly to ω^- and ω^+, as the motor angles at which the tensioner of the ith layer starts and stops being actuated. They are now defined as a function of $\Delta\omega$, but also as a function of $\xi \in [0; 1]$, already defined in section 2.2. The phase difference between two arms can be calculated as $\omega_{i+1}^+ - \omega_i^+ = \xi\Delta\omega$. For $\xi = 0$ we have $\omega_{i+1}^+ - \omega_i^+ = 0$, thus all the tensioners are actuated at the same time. In this case the SPEA becomes equivalent to a series elastic actuator with n springs in series. When $\xi = 1$ then $\omega_{i+1}^+ - \omega_i^+ = \Delta\omega$ and the tensioners are actuated one by one. When $0 < \xi < 1$ several layers can be actuated at the same time as already explained. The importance of the overlap will be detailed later. The function f_φ depends on ω_i^*, which is just a shift of ω. It can easily be checked that $\omega_i^*(\bar{\omega_i}) = -\Delta\omega/2$ and $\omega_i^*(\omega_i^+) = \Delta\omega/2$.

Next comes the output torque of the SPEA ($T_{o,\text{SPEA}}$). It is simply found by summing the contributions of all layers [27]:

$$\begin{aligned}
T_{o,\text{SPEA}} &= \sum_{i=1}^{n} T_{\text{out},i}(B_i(\omega),\, \alpha_i) \\
&= \sum_{i=1}^{n} kB_i(\omega)C\sin\alpha_i \\
&\times \left(1 + \frac{P - C + B_0 + F_0/k}{\sqrt{B_i(\omega)^2 + C^2 - 2B_i(\omega)C\cos\alpha_i}}\right) \\
&= \sum_{i=1}^{n} kB_iC\sin(\alpha_{\text{SPEA}} + \varphi_{\text{SPEA}} - \varphi_i) \\
&\times \left(1 + \frac{P - C + B_0 + F_0/k}{\sqrt{B_i^2 + C^2 - 2B_iC\cos \\ \times(\alpha_{\text{SPEA}} + \varphi_{\text{SPEA}} - \varphi_i)}}\right).
\end{aligned} \tag{10}$$

One can notice that α_i was replaced by $\alpha_{\text{SPEA}} + \varphi_{\text{SPEA}} - \varphi_i$ as $\alpha_i + \varphi_i = \alpha_{\text{SPEA}} + \varphi_{\text{SPEA}} = \Psi$. Using equation (10) the equilibrium position of the actuator in function of the motor position (hence $\varphi_{\text{SPEA}}(\omega)$) can be found by solving $T_{o,\text{SPEA}}(\varphi_{\text{SPEA}}(\omega), \alpha_{\text{SPEA}} = 0) = 0$:

$$\begin{aligned}
0 &= \sum_{i=1}^{n} kB_i(\omega)C\sin(\varphi_{\text{SPEA}} - \varphi_i(\omega)) \\
&\times \left(1 + \frac{P - C + B_0 + F_0/k}{\sqrt{B_i(\omega)^2 + C^2 - 2B_i(\omega)C \\ \cos(\varphi_{\text{SPEA}} - \varphi_i(\omega))}}\right).
\end{aligned} \tag{11}$$

A drawback of this design is that now the pretension of the springs (P) will change the relationship between the equilibrium position and the motor angle, while they were decoupled for the standard MACCEPA. The equilibrium position for two different pretension settings is shown on figure 15.

Finally, the load applied to the motor can be compared to the output torque. Knowing the equilibrium and deviation angles of each layer equation (7) can be used to find the load exerted on the motor by each layer.

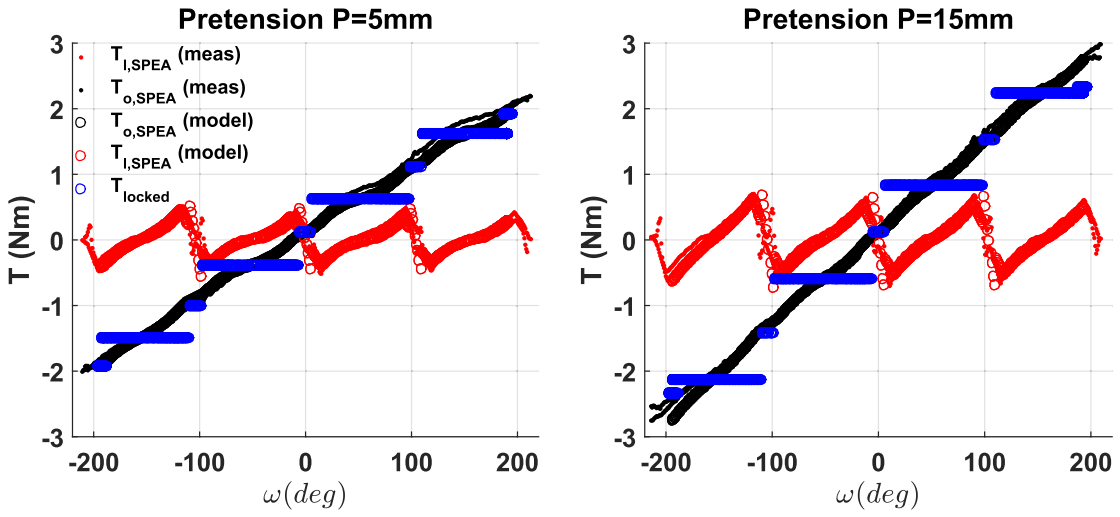

Figure 16. The load on the motor is up to four times lower than the output torque. By increasing the pretension, the stiffness is increased, and one can see that the maximum value of $T_{o,\mathrm{SPEA}}$ also increases. T_{locked} is the torque delivered by the springs that are locked (thus acting in parallel). When the tensioners are all locked, $T_{\mathrm{locked}} = T_{o,\mathrm{SPEA}}$ (see $\omega = \pm 200°$, $\omega = \pm 100°$, $\omega = 0°$) (reproduced with permission from [27], copyright 2014).

If one considers a configuration where L_l tensioners are locked on the left side, L_r tensioners are locked on the right side and A tensioners are being currently actuated, the total load on the motor ($T_{l,\mathrm{SPEA}}$) and the output torque can be expressed as follows:

$$\begin{aligned}
T_{l,\mathrm{SPEA}} &= \sum_{L_l} T_{l,i}(B_i, \alpha_i) \\
&+ \sum_{A} T_{l,i}(B_i, \alpha_i) + \sum_{L_r} T_{l,i}(B_i, \alpha_i) \\
&= \underbrace{0}_{} + \underbrace{\sum_{A} T_{l,i}(B_i, \alpha_i)}_{} + \underbrace{0}_{} \\
&\quad \text{Unit(s) locked (left)} \quad \text{Unit(s) actuated} \quad \text{Unit(s) locked (right)} \\
&= \overbrace{\sum_{L_l} T_i(B_{\mathrm{end}}, \Psi + \varphi_{\mathrm{end}})} + \overbrace{\sum_{A} T_i(B_i, \alpha_i)} \\
&+ \overbrace{\sum_{L_r} T_i(B_{\mathrm{end}}, \Psi - \varphi_{\mathrm{end}})} \\
T_{o,\mathrm{SPEA}} &= \sum_{L_l} T_i(B_i, \alpha_i) \\
&+ \sum_{A} T_i(B_i, \alpha_i) + \sum_{L_r} T_i(B_i, \alpha_i). \qquad (12)
\end{aligned}$$

By writing the load and output torques in this form, the purpose of the SPEA can be emphasized. First only the layers being actuated contribute to the load carried by the motor, while the output torque depends on both active (layers being actuated) and passive contributions (layers being locked). Furthermore, it is possible to change the passive contributions by changing the side on which the tensioners are locked.

A blocked output experiment was performed with the SPEA which is depicted in figure 16. The experiment was repeated with two different pretension settings to show the variable stiffness of the actuator.

For $\xi = 1$, the tensioners are actuated one by one, and the load torque will simply be a repetition (four times) of the torque profile of figure 14. The output torque, conversely, is the sum of the output torques of every layer. It will also be the repetition of the output torque of figure 14 but shifted to the top or to the bottom depending on how many layers are locked on the left/right side. Indeed, as $\Psi = 0$, it follows that $\alpha_i = \pm\varphi_{\mathrm{end}}$ for the blocked layers and the torque they provide is equal to $T_i(B_{\mathrm{end}}, \pm\varphi_{\mathrm{end}})$, which is constant. The total contribution of the locked layers is thus equal to $(L_l - L_r)\,T_i(B_{\mathrm{end}}, \varphi_{\mathrm{end}})$ as $T_i(B_{\mathrm{end}}, -\varphi_{\mathrm{end}}) = -T_i(B_{\mathrm{end}}, \varphi_{\mathrm{end}})$. As the tensioners are locked from one side to the other, only the quantity $(L_l - L_r)$ changes resulting in a shift of the output torque depicted in figure 14. This is also made clearer on figure 17(a) where $T_{o,\mathrm{SPEA}}$ is plotted in function of $T_{l,\mathrm{SPEA}}$. One can observe the repetition of the same pattern, but at different offsets due to the passive contributions.

For a given task, the phase difference between the arms can be selected in order, for example, to reduce the energy consumption. In the case of the blocked output experiment, the phase difference was selected such that it reduces the square of the load torque over ω (hence $\int_{\omega_1^-}^{\omega_n^+} T_{o,\mathrm{SPEA}}^2\,\mathrm{d}\omega \Big/ \int_{\omega_1^-}^{\omega_n^+} \mathrm{d}\omega$). It was already explained that the Joule losses are proportional to the square of the load and ξ was thus selected to reduce these losses. The optimization could have been done in order to directly reduce the energy for the given task, but the current selection of ξ was sufficient to demonstrate the benefits that the phase difference can bring.

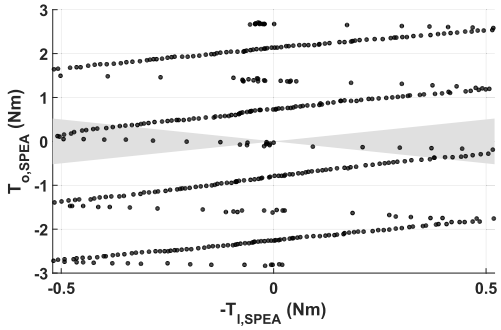

(a) $T_{o,SPEA}$ in function of $T_{l,SPEA}$ for the blocked output of Fig 16 (P=15mm). The gray area represents the zone where $|T_{o,SPEA}| < T_{l,SPEA}$. A few points lie in this zone, meaning that the load on the motor can be higher than the torque generated at the output. Nonetheless, most of the points lie outside of this zone, showing that there is indeed a load reduction.

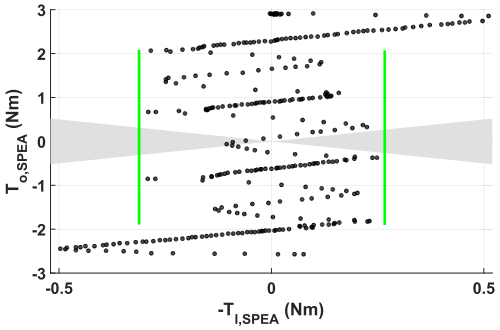

(b) Output torque in function of the load torque for the blocked output of Fig 18a (P=15mm and $\xi = 0.6$).The mean value between the forward and backward load torque is given here. The load torque is now reduced (see green lines bounding the load torque) for low output torque but is unchanged for higher torque.

Figure 17. Output torque in function of the load torque for two different phase shift in a blocked output experiment.

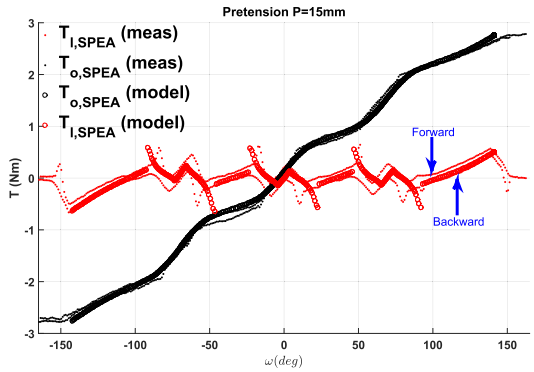

(a) Blocked output with P=15mm and $\xi = 0.6$. The maximum output torque, as load torque, are the same but the load torque over $\omega \in [-100°; 100°]$ is flatter as the load torques of the actuated layers are partially canceling each other. There are two curves for $T_{o,SPEA}$ and $T_{l,SPEA}$. One curve is given for ω going from 200° to −200° (forward) and the other for ω going from −200° to 200° (backward).

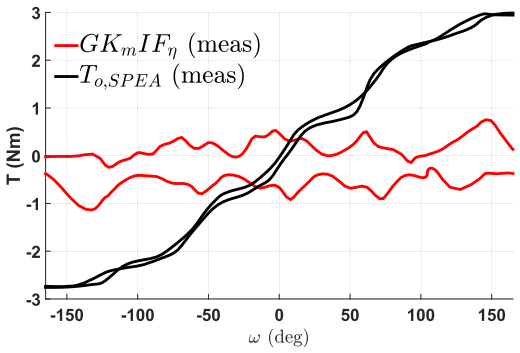

(b) Blocked output with P=15mm and $\xi = 0.6$ with a motor. An estimate of the motor torque based on the measure of the current is given. One can notice that the peaks in the motor torque correspond to the peaks in the load torque in Fig. 18a. The difference between the two torques is due to the un-modeled inertial and friction effects of the system and motor.

Figure 18. Effect of the phase difference on the torque profile.

This can be seen in figures 18(a) and 17(b) where the blocked output experiment of figure 16 is repeated for $\xi = 0.6$. One can see that the amplitude (as well as the peaks) of the load torque between $\omega \in [-100°; 100°]$ has been reduced. By changing the phase difference between the arms, there is an overlap between the unlocking and locking of the tensioners. As such, a part of the torque required to lock one tensioner is provided by the unlocking of the next one. The unlocking of the first tensioner cannot be compensated by the locking of another tensioner, and thus the torque profile for $\omega > 100$ and $\omega < -100°$ is the same as for $\xi = 1$. It can also be viewed from the energetic point of view: here the energy stored in a spring is re-used when it is being locked to unlock the next spring. In case of interaction with the output tuning ξ would thus change how the power flows from the motor to the springs and the output. This could be used advantageously to reduce the energy consumption of the motor.

Up to this point, the effect of the mechanism on the consumption of the whole actuator (thus all the losses in the electrical motor) has not been considered yet. This will be done in the next section.

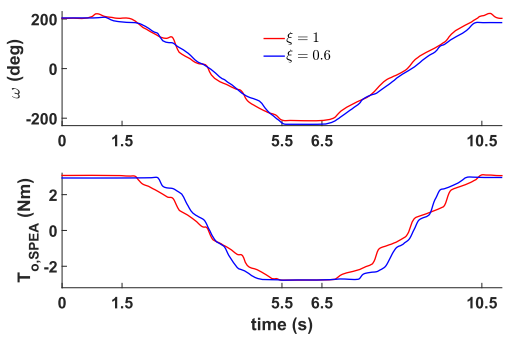

(a) Position of the motor (top) and output torque (bottom). The same trajectory was tracked for both experiments, giving matching profiles for ω. For $\xi = 0.6$ the torque goes from its maximum value to its minimum value in a shorter amount of time since the travel angle is smaller.

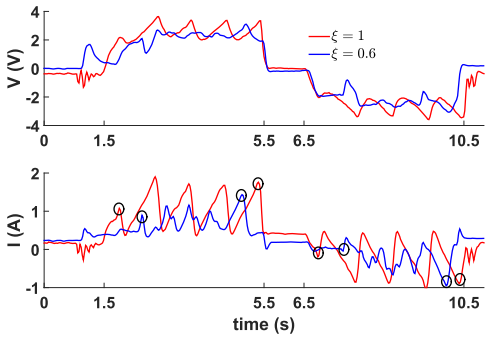

(b) Voltage and current on the motor. The sawtooth profile is very similar to figure 16 and figure 18a, which is logical, since a peak of torque will translate in a peak of current and voltage. The black circles represent the peaks of torques when the first and last tensioners are actuated.

Figure 19. Electrical measurements for a blocked output.

5. Motor consumption

In this section the consumption of the SPEA will be studied and compared with an equivalent stiff setup. It will also be investigated how the consumption is affected when tuning the parameter ξ. First the classical model of a DC motor (when the inductance is neglected) with a transmission is given:

$$\begin{aligned} JG\ddot{\omega} + \nu G\dot{\omega} &= K_m I - \frac{T_l}{GF_\eta} \\ RI &= V - K_b G\dot{\omega} \\ F_\eta &= \begin{cases} \eta & \text{if } T_l\dot{\omega} \geqslant 0 \\ 1/\eta & T_l\dot{\omega} < 0 \end{cases} \end{aligned} \tag{13}$$

J is the inertia of the motor and the transmission, ν is the motor's friction coefficient, K_m the torque constant, G the transmission ratio, η the efficiency of the transmission, R the resistance, I the current, V the voltage and K_b the speed constant. The test setup uses a SAVOX sc-0251 mg servomotor. From the data-sheet and the servomotor itself only the transmission ratio and the torque constant can be obtained: $K_m = 1.6\,\text{mNm A}^{-1}$ and $G \approx 340$. The other parameters were estimated from motors with a similar rated power (≈6W): $J = 5.7 \times 10^{-7}\text{kgm}^2$, $\nu = 12 \times 10^{-7}$ Nmsrad^{-1}, $\eta = 0.5, R = 1.6\,\Omega$.

In case of slow motion, the inertial and friction effects can be neglected, and the motor torque ($K_m I$) is equal to the load seen by the motor ($T_l F_\eta / G$). The Joule losses are then equal to $RI^2 = R(T_l F_\eta / K_m G)^2$, i.e. proportional to the square of the load. These are generally the main losses in a DC motor, and the goal of the mechanism presented in this paper is to reduce these losses. Although a blocked output experiment is just performed to study the torque angle characteristic of the actuator, it will also be used here to evaluate the electric consumption. A blocked output experiment does not produce any work at the output (since the velocity of the output link is zero) but the actuator is still required to deliver a torque and thus this can serve as a case study.

The blocked output experiment was performed for two different ξ at low speed in order to limit the dynamic contributions. The motor angle, output torque, current and voltage are depicted on figure 19. Accurately tracking the same torque profile for $\xi = 1$ and $\xi = 0.6$ was not possible with the test setup and thus only the same motor angle was tracked. Between $t = 0...1.5$ s, $t = 5.5...6.5$ s and $t > 10.5$ s the motor is still (no work is done) and the maximum/minimum torques ($\approx \pm 3$ Nm $= \pm T_{o,\max}$) are achieved as all the tensioners are locked on one side. ω goes from $-200°$ to $200°$ between $t = 1.5...5.5$ s and from $-200°$ to $200°$ between $t = 6.5...10.5$ s (tensioners are moved from side to the other). It is possible to relate the profile of the current to the torque profile of figure 18(a) (done on figure 18(b)). In particular, the peaks of current correspond to the peak of maximum torque and unlocking of the tensioners. One can also observe a forward-backward cycle on figure 18(b) similar to what was observed on figure 18(a) although it is much more pronounced on figure 18(b).

The main observation is that the amplitudes of the voltages are similar for both ξ, but the amplitude of the current is clearly lower for $\xi = 0.6$, which was expected as the load is reduced. One can notice that the first and last peaks between $t \approx 2$ s and $t \approx 5$ s for both ξ have the same amplitude (see black circles on figure 19(b)), because they both correspond to the case were the last and first tensioners are actuated alone, giving the same load and thus the same current. The voltage, as the current, is not always zero when the motor is still (see $t = 0...1.5$ s, $t = 5.5...6.5$ s and $t > 10.5$ s), which is unexpected and may reflect extra loss in the gearbox as the current and voltage are directly measured at the level of the DC motor (thus after the controller). Imprecision in the measurements

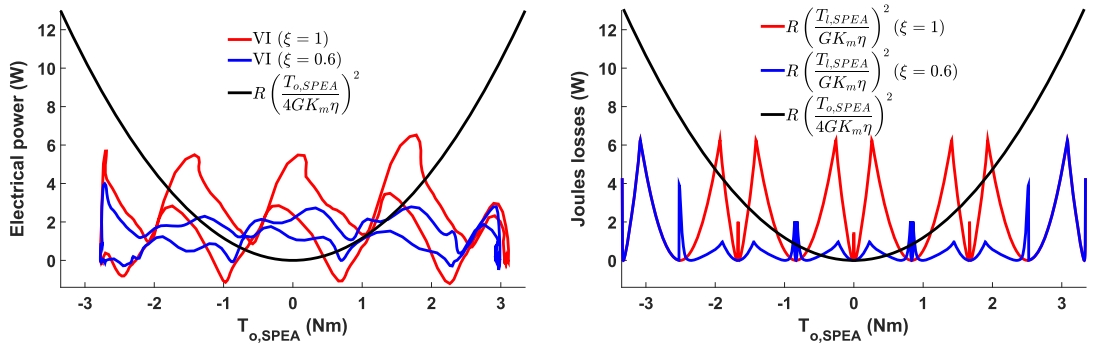

(a) Measured electrical power in function of the output torque.

(b) Modeled Joule losses in function of the output torque.

Figure 20. When $\xi = 1$, even for very low output torques the motor carry a higher load. By using a different ξ ($\xi = 0.6$) it is possible to achieve a flat region over a wide range of output torques. For $|T_{o,\text{SPEA}}| > 2.5$ Nm the power for $\xi = 1$ and $\xi = 0.6$ are superposed as only one spring is actuated.

could also be a reason. The overall behavior of the motor can still be explained from the load curve but not accurately be predicted by simply combining the model of a DC motor and the kinetostatic model of the mechanism.

Figure 20(a) gives the electrical power (so the product of the current and voltage given on figure 19(b)) in function of the output torque. The modeled Joule losses linked to the load torque for the SPEA with two different ξ are given along with the Joule losses of an equivalent stiff actuator represented by a black line (figure 20(b)). The equivalent stiff actuator carries the output torque (the motor is directly connected to the output link) but a gear ratio of four was added (without any loss of efficiency). There are two reasons: first the servomotor is not able to carry the output torque (the stall torque being 1.57 Nm) and thus an extra transmission is required. Secondly, each time a spring is locked its layer provides a fourth of the maximum load; therefore it was decided to multiply the current transmission of the servomotor by the number of layers. This way, an equivalent stiff setup is created.

As mentioned before the current profile is not the same when going forward and backward (see figure 18(b)) and so is the electrical power which explains why there are two curves for each ξ on figure 20(a). One can also notice the peaks in both figures which corresponds to the points of maximum load torque. One can see that the power of the SPEA is higher than its stiff counterpart for low torques when $\xi = 1$. For high torques, the power remains at the same level, while the power of the stiff actuator increases as it is a quadratic function of the torque. When tuning ξ for a specific task, it is possible to achieve a relatively flat power curve for a large range of output torques (from -2 to 2 Nm). For high torques again only one layer is actuated alone thus the power for $\xi = 1$ and $\xi = 0.6$ are equal. Although the shape of both figures differ (model and measurements), the peaks still occur at the same output torques. Furthermore, the power for $\xi = 0.6$ has indeed been reduced for lower torques. The energy consumed is the integral of the power. By looking at figure 20(a) it can be deduced that there is a reduction of consumption on time intervals where $T_o > |1.5|$ Nm and an increase of consumption for $T_o < |1.5|$ Nm. Considering that the goal here is to generate high torques one can foresee that the consumption of the SPEA, especially when ξ is properly tuned, will be lower than the one of a stiff actuator.

6. Conclusion and future work

In this paper, the design of a SPEA inspired by biological muscles was presented. The concept of variable recruitment of muscles units was used and combined with an intermittent mechanism to only use one motor. The design of the different parts as well as the different characteristics of one layer (kinematic, locking and kinetostatic model of the torque) were studied and validated experimentally. Next, the whole SPEA was considered and it was shown, from a simple experiment, how the load acting on the motor can be reduced. The phase difference between the different layers was introduced and electrical measurements were performed to evaluate the consumption of the actuator. It was also shown that the consumption, with respect to a stiff actuator, can be reduced, especially when tuning the phase difference. This actuator, in comparison of the previous design using mutilated gears, has several advantages such as bi-directional output torque, variable stiffness and reduced friction from the locking mechanism. In this work, only a simple task was considered, but future work should also evaluate how this actuator can cope with more challenging tasks for robotic systems. A more detailed comparison with other concepts such as SEAs, PEAs and stiff actuators could also be provided. One possibility is manipulators which could benefit greatly from a system with variable load cancellation. It

should also be studied how variable phase differences ξ_i could influence the consumption for complex tasks. The setup in this paper was built using rapid prototyping techniques such as laser-cutting and 3D printing. A more robust design with higher torque capability should be made. Electrical measurements could fit to the model better if the design of the setup was improved. Only the position control of the servomotor was used, but existing control strategies for compliant actuators can be implemented in order to also achieve better results. Currently the main limitation of the actuator is the maximum number of layers for a giving range of equilibrium angles. This is critical since, for four layers, the range is approximately reduced to $\pm 45°$. Future work should therefore consider how to tackle this problem. The actuator presented also has a higher complexity than SEAs or PEAs, which can be regarded as the price to pay to reduce the torque requirement on the motor. Considering the fast technical progress in fields of additive manufacturing this is however not considered as an obstacle. The actuator fits in the study of novel actuators capable of improving torque-to-weight ratios and energy efficiency.

Acknowledgments

This work was funded by the European Commission ERC Starting grant SPEAR (no.337596). Tom Verstraten and Glenn Mathijssen are funded by PhD Fellowship of the Research Foundation—Flanders (FWO).

References

[1] Pratt G and Williamson M 1995 Series elastic actuators *Proc. 1995 IEEE/RSJ Int. Conf. on Intelligent Robots and Systems. Human Robot Interaction and Cooperative Robots* vol 1 pp 399–406

[2] Bicchi A, Tonietti G, Bavaro M and Piccigallo M 2005 Variable stiffness actuators for fast and safe motion control *Int. J. Robot. Res.* **15** 527–36

[3] Zinn M, Khatib O, Roth B and Salisbury K 2004 Playing it safe *IEEE Robot. Autom. Mag.* **11** 12–21

[4] Garabini M, Passaglia A, Belo F, Salaris P and Bicchi A 2011 Optimality principles in variable stiffness control: the VSA hammer *IEEE Int. Conf. on Intelligent Robots and Systems* pp 3770–5

[5] Pons J 2010 Rehabilitation exoskeletal robotics *IEEE Eng. Med. Biol. Mag.* **29** 57–63

[6] Sugar T G and Holgate M 2013 Understanding speed and force ratios for compliant mechanisms *Advances in Mechanisms, Robotics and Design Education and Research* vol 14 (Berlin: Springer) pp 117–129

[7] Van Ham R, Vanderborght B, Van Damme M, Verrelst B and Lefeber D 2007 MACCEPA, the mechanically adjustable compliance and controllable equilibrium position actuator: design and implementation in a biped robot *Robot. Auton. Syst.* **55** 761–8

[8] Wolf S, Eiberger O and Hirzinger G 2011 The DLR FSJ: energy based design of a variable stiffness joint *IEEE Int. Conf. on Robotics and Automation* pp 5082–9

[9] Jafari A, Tsagarakis N G and Caldwell D G 2011 AwAS-II: a new actuator with adjustable stiffness based on the novel principle of adaptable pivot point and variable lever ratio *IEEE Int. Conf. on Robotics and Automation (ICRA)* pp 4638–43

[10] Vanderborght B *et al* 2013 Variable impedance actuators: a review *Robot. Auton. Syst.* **61** 1601–14

[11] Marden J H 2005 Scaling of maximum net force output by motors used for locomotion *J. Exp. Biol.* **208** 1653–64

[12] Semini C, Tsagarakis N G, Guglielmino E and Caldwell D G 2010 Design and experimental evaluation of the hydraulically actuated prototype leg of the HyQ robot *IEEE/RSJ Int. Conf. on Intelligent Robots and Systems* pp 3640–5

[13] Seok S, Wang A, Chuah M Y, Otten D, Lang J and Kim S 2013 Design principles for highly efficient quadrupeds and implementation on the MIT Cheetah robot *Proc.—IEEE Int. Conf. on Robotics and Automation* pp 3307–12

[14] Tsagarakis N G, Morfey S, Dallali H, Medrano-Cerda G a and Caldwell D G 2013 An asymmetric compliant antagonistic joint design for high performance mobility *IEEE Int. Conf. on Intelligent Robots and Systems* pp 5512–7

[15] Paine N, Oh S and Sentis L 2013 Design and control considerations for high performance series elastic actuators *IEEE/ASME Trans. Mechatronics* vol 19 pp 1080–91

[16] Xiu W, Ruble K and Ma O 2014 A reduced—gravity simulator for physically simulating human walking in microgravity or reduced—gravity environment *IEEE Int. Conf. on Robotics & Automation* pp 4837–43

[17] Herder J L 1998 Design of spring force compensation systems *Mech. Mach. Theory* **33** 151–61

[18] Haeufle D F B, Taylor M D, Schmitt S and Geyer H 2012 A clutched parallel elastic actuator concept: towards energy efficient powered legs in prosthetics and robotics *IEEE RAS and EMBS Int. Conf. on Biomedical Robotics and Biomechatronics* pp 1614–9

[19] Au S K, Weber J and Herr H 2009 Powered ankle—foot prosthesis improves walking metabolic economy *IEEE Trans. Robot.* **25** 51–66

[20] Towe L and Lusche S 1981 *Motor Coordination* vol 5 (New York: Springer)

[21] Mathijssen G, Lefeber D and Vanderborght B 2015 Variable recruitment of parallel elastic elements : series-parallel elastic actuators (SPEA) with dephased mutilated gears *IEEE/ASME Trans. Mechatronics* **20** 594–602

[22] van der Smagt P, Grebenstein M, Urbanek H, Fligge N, Strohmayr M, Stillfried G, Parrish J and Gustus A 2009 Robotics of human movements *J. Physiol., Paris* **103** 119–32

[23] Mathijssen G, Cherelle P, Lefeber D and Vanderborght B 2013 Concept of a series-parallel elastic actuator for a powered transtibial prosthesis *Actuators* **2** 59–73

[24] Robinson R M, Kothera C S and Wereley N M 2015 Variable recruitment testing of pneumatic artificial muscles for robotic manipulators *IEEE/ASME Trans. Mechatronics* vol 20 pp 1642–52

[25] Bryant M, Meller M a and Garcia E 2014 Variable recruitment fluidic artificial muscles: modeling and experiments *Smart Mater. Struct.* **23** 074009

[26] Mathijssen G, Schultz J, Vanderborght B and Bicchi A 2015 A muscle-like recruitment actuator with modular redundant actuation units for soft robotics *Robot. Auton. Syst.* **74** 40–50

[27] Mathijssen G, Furnémont R, Brackx B, Ham R V, Lefeber D and Vanderborght B 2014 Design of a novel intermittent self-closing mechanism for a MACCEPA-based series-parallel elastic actuator (SPEA) *IEEE/RSJ Int. Conf. on Intelligent Robots and Systems* pp 2809–14

[28] Doornbos D and Bivens S 2005 Self-closing slide mechanism with damping *US Patent* 6,848,759 (https://google.be/patents/US6848759)

[29] Hu T 2011 Self closing mechanism for drawer slides *US Patent* 8,083,304 (https://google.be/patents/US8083304)

[30] Tsagarikis N G, Jafari A and Caldwell D G 2010 A novel variable stiffness actuator: minimizing the energy requirements for the stiffness regulation *Annual Int. Conf. of the IEEE Engineering in Medicine and Biology Society* pp 1275–8